

Optical Diagnostics of Free Charge Carriers in Silicon Nanowire Arrays

Sofia P. Rodichkina,^{*} Tetyana Nychporuk, Alexander V. Pavlikov, Volodymyr Lysenko, and Victor Yu. Timoshenko

The impact of free charge carriers in arrays of silicon nanowires (SiNWs) of p- and n-type conductivities on their optical properties is probed by means of the infrared spectroscopy in attenuated total reflectance mode (IR-ATR) and Raman scattering. SiNWs are fabricated by metal-assisted chemical etching of low-doped p-type crystalline silicon (c-Si) wafers followed by thermodiffusional doping with p- and n-type impurities. The free charge carrier concentration in SiNWs is determined from their ATR spectra fitted using a model of the anisotropic effective medium with free charge carriers. The obtained data on the free charge carrier concentrations in the range of 10^{19} – 10^{20} cm^{−3} are compared with the corresponding values obtained from the Raman spectra, which are analyzed by considering the Fano effect in SiNWs, and the results of both methods are used to evaluate the electrical properties of SiNWs. The proposed optical methods to probe the electrical properties of SiNWs are discussed in view of possible applications in nanoelectronics and thermoelectric devices.

Traditionally, the electrical characterization of SiNWs is conducted using direct methods, analogous to those for bulk materials.^[2,3] The nanofabrication of electrical contacts to nanowires is performed, and the electrical conductivity of SiNWs is measured. The direct measurements of nanowires are rather complicated, and we suggest alternative optical methods for the electrical diagnostics of SiNWs. In contrast to direct measurements, the optical methods are contactless, nondestructive, and allow us to study the electrical properties of SiNWs arrays.

Optical properties of SiNWs are rather well understood. SiNWs arrays, fabricated by metal-assisted chemical etching (MACE), exhibit ultra-low reflectance in visible^[6] and infrared^[7] (IR) region as compared with bulk crystalline silicon (c-Si), which

1. Introduction

Silicon nanowires (SiNWs) are attracting research interest because of their relatively high electrical conductivity at the nanometer scale,^[1–3] which allows to apply them in nanoelectronic^[4] and sensor^[5] devices. SiNWs also exhibit low thermal conductivity that is promising for their thermoelectric applications.^[3]

decreases with nanowire length. This fact was explained by the light-trapping effect caused by light scattering in SiNW array.^[8,9] The latter effect was responsible for an enhancement of the one-phonon Raman peak in MACE-SiNW arrays compared with c-Si.^[10,11] In addition, the Raman spectra of porous MACE-SiNWs, fabricated on highly doped p- and n-type c-Si substrates, exhibited the Fano effect, related to the electron–phonon interaction, as well as the phonon confinement effect.^[12] Note that the Raman spectra of SiNWs can be strongly affected by the photoinduced heating, that was used to determine the thermal conductivity of SiNWs.^[10]

IR reflectance and Raman scattering spectroscopy have already been used to probe the free charge carriers in c-Si.^[13–15] Previously, the IR spectroscopy in attenuated total reflectance (ATR) mode was applied to porous Si (por-Si) prepared by MACE.^[16] To determine the free charge carrier concentration in por-Si, the experimental ATR spectra were fitted using the effective medium approximation for isotropic spherical nanocrystals and Drude model for free charge carriers. Using the suggested modeling, the free electron concentrations in n-type por-Si layers $\approx 10^{19}$ cm^{−3} were measured.^[16] Recently, Raman spectroscopy was applied to probe the free charge carrier concentration in p-type SiNWs in the range of 10^{19} – 10^{20} cm^{−3}.^[17] However, the data obtained both by infrared spectroscopy in attenuated total reflectance (IR-ATR) and by Raman techniques were not verified by other methods.


In this work, we apply the IR-ATR and Raman spectroscopy to probe the free charge carrier concentration in both p- and n-type

S. P. Rodichkina, Dr. A. V. Pavlikov, Prof. V. Yu. Timoshenko
Faculty of Physics
Lomonosov Moscow State University
Leninskie Gory 1, Moscow 119991, Russia
E-mail: rodichkina-s@yandex.ru

S. P. Rodichkina, Dr. T. Nychporuk, Dr. V. Lysenko
Nanotechnology Institute of Lyon
UMR CNRS 5270
INSA de Lyon
University of Lyon
Lyon F-69621, France

Dr. V. Lysenko, Prof. V. Yu. Timoshenko
PhysBio Institute
National Research Nuclear University 'MEPhI' (Moscow Engineering Physics Institute)
Kashirskoe sh. 31, Moscow 115409, Russia

Prof. V. Yu. Timoshenko
Lebedev Physical Institute of the Russian Academy of Sciences
Leninskiy Prospekt 53, Moscow 119991, Russia

 The ORCID identification number(s) for the author(s) of this article can be found under <https://doi.org/10.1002/pssa.201900670>.

DOI: 10.1002/pssa.201900670

SiNWs. The IR-ATR data are analyzed by considering SiNWs as an optically anisotropic medium. The Raman spectra are analyzed considering the Fano effect in heavily doped SiNWs. The values of free charge carrier concentration obtained by IR-ATR and Raman techniques are compared. In addition, the electrical conductivity of SiNWs is estimated using the obtained values of free charge carrier concentration.

2. Experimental Section

Initial low-doped SiNWs arrays were fabricated by the two-step MACE of low boron-doped, (100)-oriented c-Si wafers (specific resistivity of 1–10 Ω cm, free hole concentration $\approx 10^{15}$ cm $^{-3}$). At first step, Ag nanoparticles were deposited on c-Si substrates by immersing them in a mixture of aqueous solutions of [AgNO₃(0.02 M):HF(5 M)] = 1:1 for 30 s. At the second step, Ag-covered c-Si wafers were etched in a mixture of aqueous solutions of [HF(5 M):H₂O₂(30%)] = 10:1 for 5–15 min to obtain SiNWs with different lengths. The residual Ag nanoparticles were removed in 65% HNO₃ for 15 min, and SiNWs arrays were rinsed in deionized water and dried in air. Fabricated SiNWs arrays were additionally doped with p-type (boron) and n-type (phosphorus) impurities. For this, a drop ≈ 0.1 mL of commercial spin-on dopant solution (Emulsitone Chemicals, LLC.) was deposited on SiNWs and spin coated at a rotation speed of 3000 rpm and dried at about 200 °C for 10 min. Then, the samples were annealed at about 1000 °C for 1 min using the rapid thermal annealing (RTA) device (Addax 1000, Meylan, France). Residual dopant and surface oxide were removed from SiNW surface in an aqueous solution of [HF(48%):C₂H₅OH] = 1:9 for 10 min, and SiNWs were cleaned with ethanol and dried in air. The presented procedure of the fabrication of highly doped SiNWs allows to overcome the limitations of traditional MACE on highly doped c-Si substrates, for which the formation of porous SiNWs^[18] or por-Si^[19] was reported.

Structural properties of SiNWs were studied using a Carl Zeiss SUPRA 40-30-87 scanning electron microscope (SEM). IR spectra were measured using a Bruker Vertex 70/80 Fourier-transform IR spectrometer in ATR mode with a single-reflection germanium (Ge) prism (45°), and mechanical contact between SiNWs sample and ATR crystal was applied until its following enhancement led to no changes in the measured spectra. Raman spectra were measured using Horiba HR 800 and LabRAM Aramis micro-Raman spectrometers with 632.8 and 473 nm excitation, correspondingly.

Figure 1 shows the SEM images of investigated SiNW samples. The samples consist of vertically aligned Si nanowires on the c-Si substrate. The mean diameter of SiNWs is of 100–300 nm, and the length is of 4–15 μ m. The mean diameter of SiNWs was found to slightly increase with their length, that is explained by a redeposition of Ag nanoparticles during etching, which leads to partial porosification and dissolution of SiNW tips. The porosity of SiNWs, determined from the top-view SEM images as a ratio of the number of dark pixels (brightness less than 50%) to the total ones, is $75 \pm 5\%$ for all samples. A comparison of SEM images before and after the additional doping revealed no significant changes in the SiNWs morphology after the doping procedure.

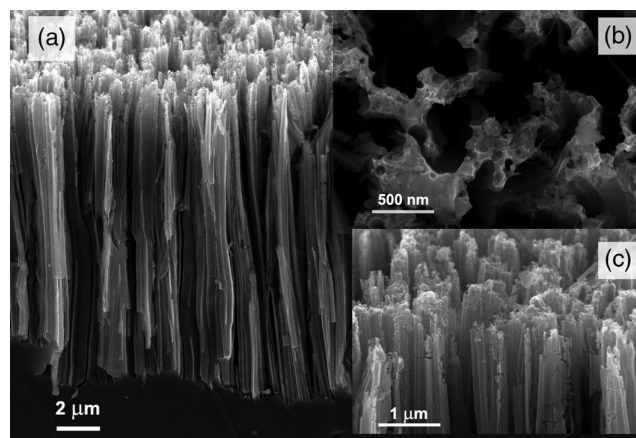


Figure 1. a) Cross-sectional and b) top-view SEM images of p-type-doped SiNWs with the length of 15 μ m. c) Magnified image of SiNWs tips.

3. IR Spectroscopy of SiNWs Arrays

3.1. Modeling of the IR-ATR Response in Anisotropic Medium

Let us consider a plane monochromatic electromagnetic wave falling on an uniaxial anisotropic crystal with an optical axis perpendicular to a surface of crystal, as shown in Figure S1, Supporting Information. The coordinate system is chosen in such a way that the z-axis is perpendicular to the sample surface (and parallel to the optical axis) and directed inside the sample, and the xz-plane represents the plane of incidence of light. The light falls from the transparent medium, which represents an ATR (Ge) crystal and is characterized by a refractive index n_{Ge} .

ATR signal measured for nonpolarized light is given by the following expression

$$R_{ATR} = (R_s + R_p)/2 \quad (1)$$

where $R_{s,p}$ is the reflectance for s- and p-polarized light, correspondingly.^[20]

In our case $R_{s,p}$ can be expressed in the following way

$$R_s = \frac{\left| \frac{\omega}{c} n_{Ge} \cos \theta - k_{zo} \right|^2}{\left| \frac{\omega}{c} n_{Ge} \cos \theta + k_{zo} \right|^2} \quad (2)$$

$$R_p = \frac{\left| \frac{\omega}{c} \varepsilon_{\perp} \cos \theta - n_{Ge} k_{ze} \right|^2}{\left| \frac{\omega}{c} \varepsilon_{\perp} \cos \theta + n_{Ge} k_{ze} \right|^2} \quad (3)$$

where ω is the frequency of the incident light, c is the speed of light, θ is the angle of light incidence, and $k_{zo,e}$ are the z-components of the light wave vector inside the sample for the ordinary and extraordinary rays, correspondingly, which are given by

$$k_{zo} = \frac{\omega}{c} \sqrt{\varepsilon_{\perp} - n_{Ge}^2 \sin^2 \theta} \quad (4)$$

and

$$k_{ze} = \frac{\omega}{c} \sqrt{\varepsilon_{\perp} - \frac{\varepsilon_{\parallel}}{\varepsilon_{\perp}} n_{Ge}^2 \sin^2 \theta} \quad (5)$$

where $\epsilon_{\perp,\parallel}$ are the dielectric constants of an uniaxial anisotropic medium (see Section 2 in Supporting Information).

To describe the dielectric function of SiNWs array, the latter can be considered within the effective medium approximation. SiNW array consists of doped Si nanocrystals and air, and in the effective medium approximation, it represents an anisotropic uniaxial medium with dielectric constants given by the generalized Bruggeman formula, as follows

$$f_A \frac{\epsilon_{\perp,\parallel} - \epsilon_A}{\epsilon_{\perp,\parallel} + L_{\perp,\parallel}(\epsilon_A - \epsilon_{\perp,\parallel})} + f_{nc} \frac{\epsilon_{\perp,\parallel} - \epsilon_{nc}}{\epsilon_{\perp,\parallel} + L_{\perp,\parallel}(\epsilon_{nc} - \epsilon_{\perp,\parallel})} = 0 \quad (6)$$

where $f_A = p$, $f_{nc} = (1 - p)$ are the volume fraction of air and Si nanocrystals in SiNWs array; correspondingly, p is the porosity of SiNWs array, ϵ_A and ϵ_{Si} are the dielectric constants of air and Si nanocrystals, correspondingly.^[21] In Equation (6) for anisotropic uniaxial medium, one should consider $L_{\perp} = 1/2$ and $L_{\parallel} = 0$. The generalized Bruggeman formula, given by Equation (6), is also valid for an isotropic medium, such as por-Si, in this case, $L_{\perp} = L_{\parallel} = 1/3$.

The dielectric constant of Si nanocrystals can be described by the Drude model as follows

$$\epsilon_{nc} = 11.7 - \frac{\omega_p^2}{\omega^2 + i\omega g} \quad (7)$$

where ω_p is the plasma frequency and g is the damping constant.^[13] To consider the additional surface scattering of charge carriers in nanocrystals, the latter can be represented as follows

$$g = g_0 \left(1 + \frac{g_1}{\omega} \right) \quad (8)$$

where g_0 is the bulk damping rate and g_1 is the surface damping rate parameter, whereas the surface damping rate is described by the term $g_0 g_1 / \omega$.^[16]

Overall, Equation (1)–(8) describes the ATR spectra for SiNWs using the parameters p , ω_p , g_0 , and g_1 . Note that, Equation (2) and (3) is valid both for anisotropic (SiNWs) and isotropic medium (por-Si), and the corresponding dielectric constants in both cases can be found using Equation (6). IR-ATR spectroscopy allows us to determine the parameters ω_p , g_0 , and g_1 for Si nanostructures by fitting the ATR spectra, whereas the porosity is usually known from other methods (e.g., SEM or gravimetric analysis). The free charge carrier concentration (N) in Si nanocrystals can be calculated as $N = \epsilon_0 m \omega_p^2 / e^2$, where ϵ_0 is the permittivity of free space, e is the electron charge, and m is the effective mass of charge carriers. $m = 0.26 m_0$ and $0.37 m_0$ for electrons and holes in c-Si, correspondingly, where m_0 is the free-electron mass.

Figure 2 shows the calculated spectra of ATR reflectance and absorption coefficient for highly doped SiNW arrays. The absorption coefficient was calculated as $\alpha = 2\omega / c^* \text{Im}\sqrt{\epsilon}$. As one can see from the figure, the values of $-\ln(R_{\text{ATR}})$ for SiNWs in the case of nonpolarized light are about two times higher than those for similar por-Si layers, that is related solely to the shape of Si nanocrystals (Equation (6)). An increase in the free charge carrier concentration in por-Si or SiNWs leads to an increase in free charge carrier absorption (α) and $-\ln(R_{\text{ATR}})$ (Figure S2 in

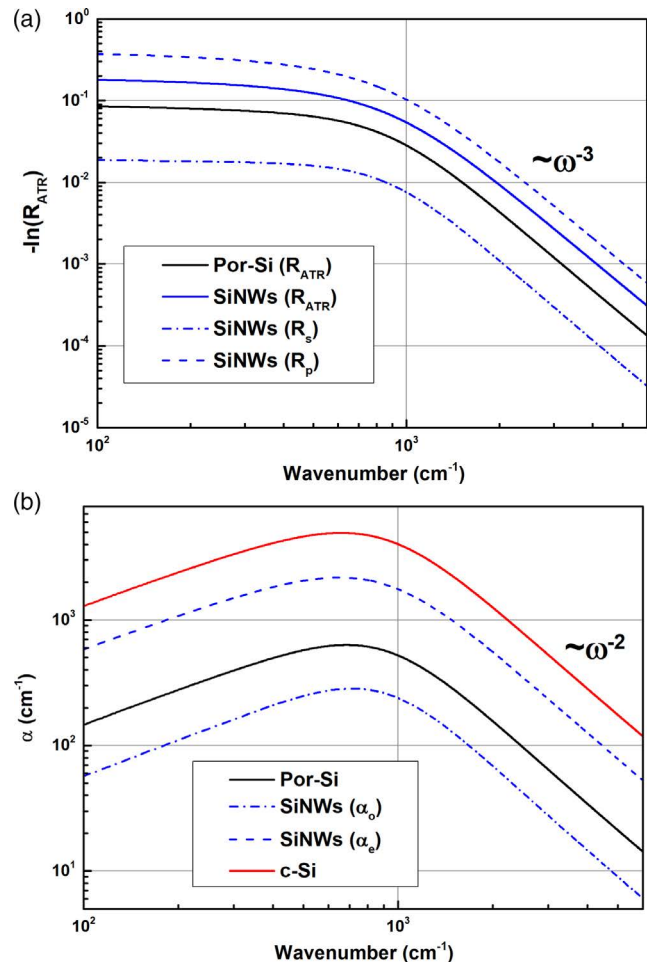


Figure 2. a) Calculated ATR spectra for p-type anisotropic medium (SiNWs) for s-, p-, and nonpolarized light (blue dash-dotted, dashed, and solid lines, correspondingly), as well as for isotropic medium (por-Si) for nonpolarized light (black solid line) (b) calculated spectra of absorption coefficient for SiNWs for ordinary and extraordinary ray (blue dash-dotted and dashed line, correspondingly), as well as for por-Si and c-Si (black and red solid lines, correspondingly). The calculation parameters both for SiNWs and por-Si are: $p = 0.75$, $\omega_p = 2000 \text{ cm}^{-1}$, $g_0 = 500 \text{ cm}^{-1}$, $g_1 = 1000 \text{ cm}^{-1}$, and $N = 1.6 \times 10^{19} \text{ cm}^{-3}$.

Supporting Information). Thus, the same values of $-\ln(R_{\text{ATR}})$ correspond to higher values of N in the case of por-Si than in the case of SiNWs. Note that, the similarity between the spectra of $-\ln(R_{\text{ATR}})$ and α allows us to compare the absorption of different SiNW arrays directly from the ATR spectra.

From Figure 2, it is shown that anisotropic SiNW arrays demonstrate an optical dichroism under polarized light with a ratio of α_e / α_o and $\ln(R_p) / \ln(R_s)$ of about 10, where α_o and α_e are the absorption coefficients of SiNW arrays for the ordinary and extraordinary rays, respectively, and R_s and R_p are the ATR reflectance under s- and p-polarized light, correspondingly.

Figure 3 shows the calculated values of the effective light penetration depth (d_{eff}) for SiNWs and por-Si, which is defined similarly to Beer–Lambert law: $-\ln(R_{\text{ATR}}) = \alpha d_{\text{eff}}$. As shown in Figure 3, d_{eff} for highly doped SiNWs and por-Si decreases with

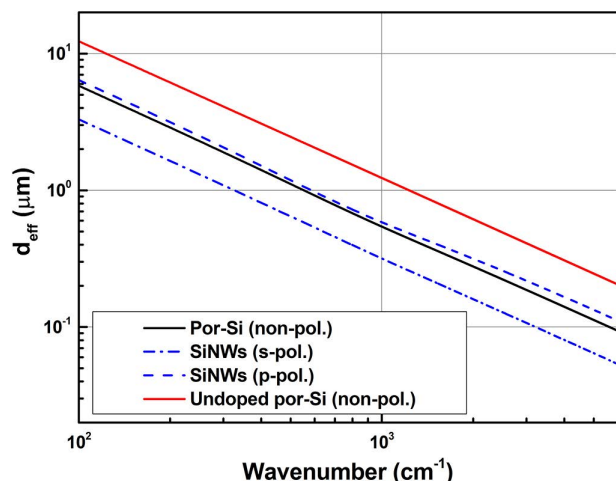


Figure 3. Calculated effective light penetration depth for s- and p-polarized incident light for p-type highly doped SiNWs (dash-dotted and dashed lines, correspondingly), and for nonpolarized incident light for doped and undoped por-Si (black and red solid lines, correspondingly).

the light frequency, and it is $\approx 1 \mu\text{m}$ at 500 cm^{-1} and $\approx 0.1 \mu\text{m}$ at 2000 cm^{-1} . In addition, d_{eff} for both doped and undoped samples can be approximated by ω^{-1} in the whole studied wavenumber range. For undoped por-Si, an analytical expression $d_{\text{eff}} = C/\omega$ can be obtained, where C is the coefficient which depends on the material of the sample and ATR prism and light incidence angle.^[22,23]

It is important to note the asymptotics for $-\ln(R_{\text{ATR}})$ and α at high wavenumbers. In particular, $\alpha \approx \omega^{-2}$ both for c-Si and Si nanostructured layers (Figure 2b), which can be explained considering that the only absorption mechanism is the free charge carrier absorption as well as Drude model (Equation (7)). The spectra of $-\ln(R_{\text{ATR}})$ exhibit the ω^{-3} asymptotics at high wavenumbers (Figure 2a). This asymptotics can be explained considering both the Drude model for Si nanocrystals and asymptotics of $d_{\text{eff}} \approx \omega^{-1}$.

3.2. Experimental Results on the IR-ATR Diagnostics

IR-ATR spectroscopy, which uses an evanescent mode of penetrated light, allows us to minimize light scattering in Si nanostructures compared with traditional reflectance geometry. **Figure 4** shows the experimental spectrum of $-\ln(R_{\text{ATR}})$ for highly doped SiNW arrays and its fits using Equation (1)–(8) with various parameters. As shown in the figure, the spectrum can be well fit using the effective medium approximation at low wavenumbers, whereas it can not be approximated with $\approx \omega^{-3}$ asymptotics, typical for our model (Figure 2), at high wavenumbers. This fact is explained by an effect of light scattering in SiNW arrays, that is negligible at low wavenumbers and increases with increasing the light wavenumber. Lower experimental values of $-\ln(R_{\text{ATR}})$ than those calculated in the model can be explained by the lower effective light absorption of SiNWs due to backscattering of the light, as well as by a change in the spectral dependence of α and d_{eff} due to light scattering. The observed light scattering effect on $-\ln(R_{\text{ATR}})$ spectra was not observed

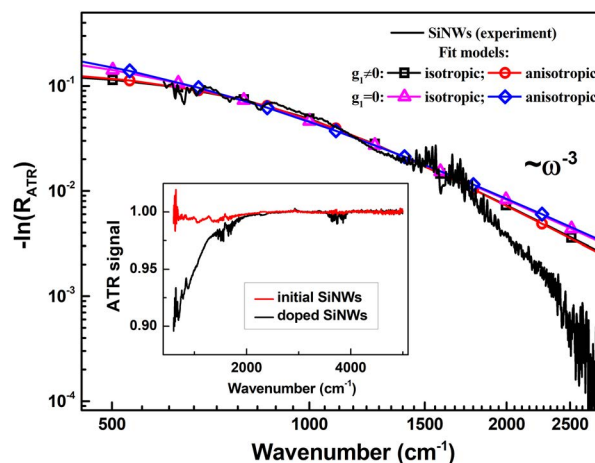


Figure 4. Spectrum of $-\ln(R_{\text{ATR}})$ for p-type-doped SiNWs array and its fitting using the anisotropic model with and without surface scattering of free charge carriers (red and blue lines, correspondingly), as well as the isotropic model with and without hole-surface scattering (magenta and black lines, correspondingly). The inset shows the ATR spectra for this SiNWs array before and after the additional doping. SiNWs length is $4 \mu\text{m}$.

for R_{ATR} (see inset in Figure 4) due to the small absolute divergence between $-\ln(R_{\text{ATR}})$ and $\approx \omega^{-3}$ approximation. Note that the effect of light scattering on IR spectra for por-Si, which was strong in specular reflectance geometry due to rather a large nanocrystal size of $\approx 100 \text{ nm}$, was negligible in ATR geometry.^[16]

Solid lines in Figure 4 show the fits of the ATR spectrum for SiNWs using the anisotropic and isotropic models, fit parameters are shown in **Table 1**. The fitting curves for anisotropic or isotropic models coincide, whereas the values of free charge carrier concentration (N), obtained using the isotropic model, are about 1.5 times larger than those for anisotropic models. This difference is explained by the different dielectric constants for isotropic and anisotropic effective media due to different shapes of Si nanocrystals (Figure 2). Then, the values of N , obtained for the surface scattering rate parameter $g_1 \neq 0$ and $g_1 = 0$, coincide within the experimental error. The values of g_0 are higher in the case when $g_1 = 0$, which is consistent with Equation (8). Note that all the discussed models give the same order of N for SiNWs array; thus, a simpler isotropic model can be used to estimate the order of N in SiNWs. The error bars for N in the IR-ATR method are mainly due to the error bars for the porosity of the sample. Considering both the error bars for

Table 1. Sample parameters obtained from the experimental data and from modeling of IR-ATR spectra for SiNWs using anisotropic and anisotropic effective medium approximations.

Fit model	p	ω_p [10^3 cm^{-1}]	g_0 [10^3 cm^{-1}]	g_1 [10^3 cm^{-1}]	N [10^{19} cm^{-3}]
Isotropic		2.5	0.6	0.6	2.6
Anisotropic	0.75	1.9	0.4	1.5	1.5
Isotropic ($g_1 = 0$)		2.5	1.0	0	2.5
Anisotropic ($g_1 = 0$)		1.9	0.8	0	1.4

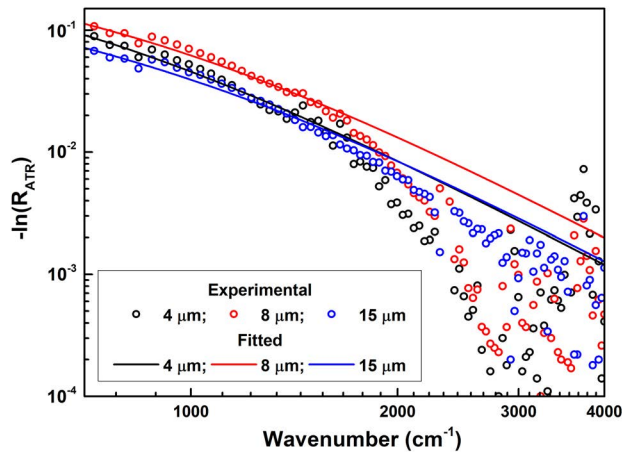


Figure 5. Experimental spectra (points) and fitting (lines) of the ATR signal ($-\ln(R_{\text{ATR}})$) for p-type highly doped SiNWs with different lengths. The fitting was done using Equation (1)–(8) considering $g_1 \neq 0$.

Table 2. Free charge carrier concentration in p-type SiNWs of different lengths obtained from the modeling of the IR-ATR spectra of SiNWs considering the anisotropic effective medium and $g_1 \neq 0$, as well as from the Raman spectra using the Fano peak half width.

Length [μm]	N [10^{19} cm^{-3}]		
	Raman	IR-ATR	IR-ATR ($p = 0.9$)
4	4.2	1.4	4.6
8	8.3	1.9	6.2
15	7.9	1.2	4.0

porosity of 5% and the inaccuracy of fitting, the total error bars for N in the IR-ATR method are estimated about 20%.

Figure 5 shows the experimental ATR spectra for p-type highly doped SiNWs of different lengths and their fit using the anisotropic model with $g_1 \neq 0$. For all SiNW lengths, the good fit is observed at low wavenumbers, whereas at high wavenumbers, the discrepancy between experiment and modeling is seen, explained by the influence of light scattering. The values of N , determined from the fit of the spectra, are shown in **Table 2**. The free hole concentration in SiNWs is $\approx 10^{19} \text{ cm}^{-3}$, which indicates the effectiveness of the proposed doping procedure for SiNWs arrays with length about 1–10 μm . The dependence of SiNW doping level on their length will be explained in the following sections.

4. Raman Spectroscopy of SiNWs Arrays

Determination of N in SiNWs using Raman spectroscopy is based on the dependence of Fano effect on free hole concentration. The Fano effect is due to the interplay between the one-phonon and electron Raman scattering in SiNWs,^[24] and the following dependence of the Raman peak half width (Γ) on N was found for p-type c-Si: $\Gamma = -1.8 + 3.8N^{1/3}$, where Γ and N are given in cm^{-1} and cm^{-3} , correspondingly.^[17] This formula is valid for $N = 10^{19}$ – 10^{20} cm^{-3} and does not depend on laser wavelength. It can be used for Si nanostructures with a diameter

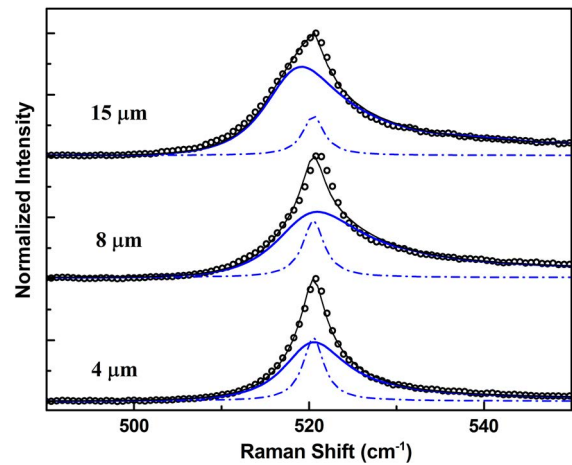


Figure 6. Normalized Raman spectra for p-type highly doped SiNWs with different lengths (circles). Blue lines correspond to the Raman peaks for doped SiNWs (solid lines) and c-Si substrate (dash-dotted lines). Black solid lines show the total fit of the Raman spectra for SiNWs samples.

more than 10 nm, for which the the quantum confinement of phonons or electrons is not observed.^[12,25]

Figure 6 shows one-phonon Raman spectra for the highly doped SiNW samples similar to the one in **Figure 5**. The Raman spectra for SiNW samples were deconvoluted to the asymmetric Fano peak and Lorentzian peak, corresponding to the doped SiNWs and c-Si substrate, respectively (**Figure 1**). Note that the Raman peak for undoped SiNWs coincides with the one for c-Si substrate due to the absence of phonon confinement effect. Analysis of the spectral broadening of the Raman peak for highly doped SiNWs allowed us to estimate $N \approx 10^{19} \text{ cm}^{-3}$ (**Table 2**). The error bars for the Raman scattering method were estimated to be about 10%. The excitation depth in SiNWs is $\approx 10 \mu\text{m}$ for 632.8 nm excitation.^[17]

5. Comparison of IR-ATR and Raman Techniques

The same order of free hole concentration estimated using the IR-ATR and Raman methods indicates the optical methods are well applicable for the express diagnostics of electrical properties of SiNWs. At that, as shown in **Table 2**, the IR-ATR spectroscopy underestimates the values of N about four times in comparison with the Raman method. This difference can be associated with the porous morphology of the top of SiNWs (**Figure 1**). As the SiNW diameters are smaller at SiNW tips, the actual porosity of SiNW layers in contact with ATR crystal is higher than that measured by SEM. This result is particularly important for SiNWs, fabricated by Ag-assisted MACE, for which SiNWs with rough surfaces are usually obtained.^[26] SiNWs fabricated, for example, by Au-assisted MACE or reactive-ion etching usually exhibit no diameter variation along nanowires,^[27,28] and the IR-ATR method results should be more accurate for such SiNWs arrays. The Raman scattering method in application to SiNWs does not have such a limitation, as the Raman peak for SiNWs with a diameter more than 10 nm is independent of their shape and porosity of SiNW arrays.

It is interesting to compare the values of N , obtained by Raman and IR-ATR techniques, assuming a high porosity at SiNW tips ($p = 0.9$, see Table 1). In this case, the values of N , obtained using the IR-ATR and Raman methods, are close to each other for 4 μm SiNWs, and the difference increases with the length of SiNWs. Considering that the porosity of SiNW tips increases during etching, the aforementioned fact is consistent with our explanation of the inaccuracy of the IR-ATR method due to the high porosity of the SiNW arrays' tips.

6. Particularities for n-Type SiNWs

Figure 7a shows an application of the IR-ATR method on n-type moderately doped SiNWs. The experimental ATR spectra and modeling (Equation (1)–(8)) are similar for n- and p-type SiNWs, which demonstrates that the IR-ATR method is not sensitive to the type of free charge carriers. The fit of the ATR spectra for moderately doped n-type SiNWs using the anisotropic model with $g_1 \neq 0$ is good in the entire wavenumber range, which was not the case for highly doped p-type SiNWs (Figure 5). This fact can be explained by weaker light scattering in SiNWs arrays with

lower N . Indeed, as the conditions of total reflectance are broken for doped SiNWs, the transmitted light wave in SiNW arrays has a nonzero energy flux along z -axis. The latter increases with N of SiNWs, which leads to the stronger scattering of the transmitted wave in SiNW arrays; however, an increase in N leads also to an increase in free carrier absorption, that suppresses light scattering. This mechanism is not described in the model equation (1)–(8); however, it can be ignored for low wavenumbers, where the effective medium approximation describes well the ATR spectra for SiNWs. Note that both for n- and p-type-doped SiNWs, the model with $g_1 \neq 0$ better describes the ATR spectra than the one with $g_1 = 0$, which indicates a strong interaction of free charge carriers with nanowire surface.

The free electron concentration in n- and p-type SiNWs after deposition of spin-on dopant is $\approx 10^{18}$ and 10^{19} cm^{-3} , correspondingly. The difference in N is related to the spin-on dopant solutions, as well as low p-type doping of initial SiNWs. Highly n-type-doped SiNWs ($N \approx 10^{19} \text{ cm}^{-3}$) were obtained using several depositions of spin-on dopant before RTA; however, in this case, a residual polymer film that does not dissolve in HF was formed on SiNW tops. This film affects the dielectric constant of SiNW arrays; thus, highly doped n-type SiNWs were studied only by Raman spectroscopy.

Figure 7b shows a comparison of the normalized Raman spectra for n-type highly doped SiNW and c-Si substrates. The Fano-like line shape with antiresonance at the high wavenumber side, seen for SiNWs, is consistent with n-type doping.^[29] As the Fano asymmetry in p-type doping results in antiresonance at low wavenumbers,^[24] the Raman method, in contrast to IR-ATR, allows us to distinguish the type of free charge carriers in SiNWs. The Fano effect for n-type c-Si, unlike p-type c-Si, can occur only if $N > 5 \times 10^{19} \text{ cm}^{-3}$,^[14,29] that is due to the fact that the overlap between energies of the one-phonon and interconduction-band electron transitions in c-Si can take place only if the Fermi level is above a rather high critical value.^[14,29] Moreover, the Fano effect in n-type c-Si is much weaker than in p-type c-Si due to the smaller electron–phonon interaction matrix element in the case of n-type SiNWs than for p-type SiNWs.^[29] Thus, one can conclude that free electron concentration in highly doped n-type SiNWs is higher than $5 \times 10^{19} \text{ cm}^{-3}$, but the precise determination of N is complicated.

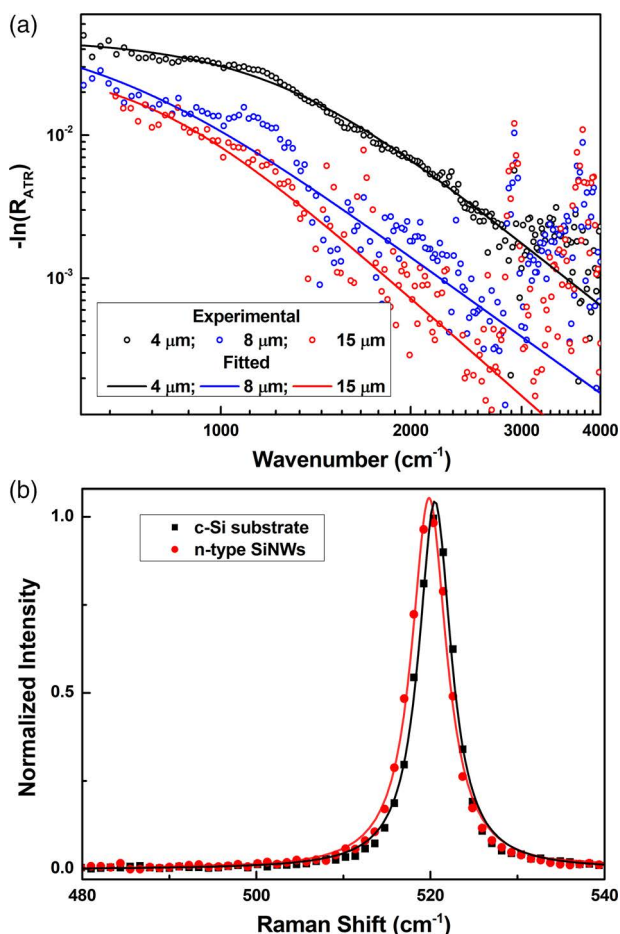


Figure 7. a) Experimental spectra (points) and fitting (lines) of the ATR signal ($-\ln(R_{\text{ATR}})$) for n-type-doped SiNWs with different lengths. The fitting was done using Equation (1)–(8) considering $g_1 \neq 0$. b) Normalized Raman spectra for highly doped n-type SiNWs and of initial c-Si substrate.

7. Estimation of the Electrical Resistivity of SiNWs

The electrical resistivity of SiNWs (ρ) can be estimated using the expression $1/\rho = eN\mu$, where e is the electron charge and μ is the free charge carrier mobility. In our case, the free hole concentration is known from the optical methods, and the free charge carrier mobility in SiNWs with $N > 10^{18} \text{ cm}^{-3}$ and diameter more than 20 nm can be considered the same as in bulk c-Si.^[30,31] A minor role of the surface scattering of free charge carriers on μ in SiNWs is explained by their small mean free path with respect to the nanowire diameter due to impurity scattering. Note that, at the same time, the phonon transport along SiNWs is significantly suppressed by the surface scattering of phonons.^[3,30]

It is important to emphasize that in SiNWs with a diameter of 20–70 nm, the free charge carrier concentration can be lower than the impurity concentration due to donor deactivation, which represents an increase in the impurity ionization energy in nanocrystals because of the dielectric mismatch between the nanocrystal and the ambient, as well as due to the surface depletion of charge carriers caused by interface states.^[32] This effect should be considered when using, for example, secondary ion mass spectrometry, which measures the impurity concentration, to estimate ρ of SiNWs.

The estimated electrical resistivity is 1.5–2.7 m Ω cm for highly doped p-type SiNWs and about 10 and 1 m Ω cm for moderately and highly doped n-type SiNWs, respectively. The high electrical conductivity of SiNWs after additional spin-on doping makes them interesting for applications in nanoelectronics and thermoelectricity.

8. Conclusions

The optical methods of IR and Raman spectroscopy were applied for the contactless diagnostics of free charge carriers in SiNW arrays. Highly doped p- and n-type SiNWs were fabricated by metal-assisted chemical etching of low-doped p-type c-Si wafers and additionally doped with p- or n-type impurities using the spin-on dopant solutions and RTA.

The IR-ATR spectroscopy was used to probe the free charge carrier concentration both in n- and in p-type SiNWs in the range of 10^{18} – 10^{20} cm $^{-3}$. The effect of light scattering on the ATR spectra of SiNWs arrays was shown to be negligible, and the latter were described based on anisotropic effective medium approximation and Drude model for free charge carriers. However, the values of N for MACE-SiNWs were underestimated about four times due to the high porosity of SiNW tops in contact with the ATR crystal.

Raman scattering spectroscopy was applied to precisely probe the free charge carrier in p-type highly doped SiNWs in the range of 10^{19} – 10^{20} cm $^{-3}$. The Fano effect for one-phonon and electron Raman scattering was shown to strongly modify the Raman peak for p-type SiNWs, and the free hole concentration in SiNWs was determined using the Fano peak half width. For n-type SiNWs, the Fano effect was weak, and it could be used only to distinguish the high doping level above 5×10^{19} cm $^{-3}$.

The electrical resistivity of SiNWs was estimated using the determined free charge carrier concentration and the bulk free charge carrier mobility, which was justified by a relatively weak surface scattering of free charge carriers in highly doped SiNWs as compared with the impurity scattering. The low electrical resistivity, ≈ 1 m Ω cm for additionally doped p- and n-type SiNWs, makes them interesting for nanoelectronics and thermoelectric applications. The proposed optical methods are important for the contactless diagnostics of electrical properties of various Si nanostructures for nanoelectronics, thermoelectrics, and sensor applications.

Supporting Information

Supporting Information is available from the Wiley Online Library or from the author.

Acknowledgements

This work was partially supported by the Ministry of Science and High Education of the Russian Federation (project no.16.2969.2017/4.6) and by the MEPhI Academic Excellence Project (contract no. 02.a03.21.0005). S.P. Rodichkina acknowledges the “Vernadski” scholarship program of the French Embassy in Russia.

Conflict of Interest

The authors declare no conflict of interest.

Keywords

attenuated total reflectance, free charge carriers, infrared spectroscopy, optical diagnostics, Raman spectroscopy, silicon nanowires

Received: August 15, 2019

Revised: November 28, 2019

Published online:

- [1] V. Schmidt, J. Wittemann, U. Gosele, *Chem. Rev.* **2010**, *110*, 361.
- [2] J. Kim, Y. Hyun, Y. Park, W. Choi, S. Kim, H. Jeon, T. Zyung, M. Jang, *J. Nanosci. Nanotechnol.* **2013**, *13*, 6416.
- [3] A. I. Hochbaum, R. Chen, R. D. Delgado, W. Liang, E. C. Garnett, M. Najarian, A. Majumdar, P. Yang, *Nature* **2008**, *451*, 163.
- [4] Y. Cui, Z. Zhong, D. Wang, W. U. Wang, C. M. Lieber, *Nano Lett.* **2003**, *3*, 149.
- [5] I. Park, Z. Li, A. P. Pisano, R. S. Williams, *Nanotechnology* **2009**, *21*, 015501.
- [6] I. Leontis, M. A. Botzakaki, S. N. Georga, A. G. Nassiopoulou, *ACS Omega* **2018**, *3*, 10898.
- [7] M. Lajvardi, H. Eshghi, M. Ghazi, M. Izadifard, A. Goodarzi, *Mater. Sci. Semicond. Process.* **2015**, *40*, 556.
- [8] Y. Liu, G. Ji, J. Wang, X. Liang, Z. Zuo, Y. Shi, *Nanoscale Res. Lett.* **2012**, *7*, 663.
- [9] S. Kato, Y. Kurokawa, Y. Watanabe, Y. Yamada, A. Yamada, Y. Ohta, Y. Niwa, M. Hirota, *Nanoscale Res. Lett.* **2013**, *8*, 216.
- [10] S. Rodichkina, L. Osminkina, M. Isaiev, A. Pavlikov, A. Zoteev, V. Georgobiani, K. Gonchar, A. Vasiliev, V. Y. Timoshenko, *Appl. Phys. B* **2015**, *121*, 337.
- [11] L. A. Osminkina, K. A. Gonchar, V. S. Marshov, K. V. Bunkov, D. V. Petrov, L. A. Golovan, F. Talkenberg, V. A. Sivakov, V. Y. Timoshenko, *Nanoscale Res. Lett.* **2012**, *7*, 1.
- [12] S. K. Saxena, R. Borah, V. Kumar, H. M. Rai, R. Late, V. Sathe, A. Kumar, P. R. Sagdeo, R. Kumar, *J. Raman Spectrosc.* **2016**, *47*, 283.
- [13] W. Theiß, *Surface Sci. Rep.* **1997**, *29*, 91.
- [14] V. Magidson, R. Beserman, *Phys. Rev. B* **2002**, *66*, 195206.
- [15] R. Beserman, T. Bernstein, *J. Appl. Phys.* **1977**, *48*, 1548.
- [16] S. P. Rodichkina, T. Nychporuk, A. Pastushenko, V. Y. Timoshenko, *Physica Status Solidi* **2018**, *12*, 1800224.
- [17] S. P. Rodichkina, T. Nychporuk, A. V. Pavlikov, V. Lysenko, V. Y. Timoshenko, *J. Raman Spectrosc.* **2019**, *50*, 1642.
- [18] T. Zhang, S. Wu, J. Xu, R. Zheng, G. Cheng, *Nano Energy* **2015**, *13*, 433.
- [19] H. Han, Z. Huang, W. Lee, *Nano Today* **2014**, *9*, 271.
- [20] L. D. Landau, J. Bell, M. Kearsley, L. Pitaevskii, E. Lifshitz, J. Sykes, *Electrodynamics of Continuous Media*, Elsevier **2013**.
- [21] D. Schmidt, M. Schubert, *J. Appl. Phys.* **2013**, *114*, 083510.
- [22] N. Harrick, *J. Opt. Soc. Am.* **1965**, *55*, 851.
- [23] W. N. Hansen, *Spectrochim. Acta* **1965**, *21*, 815.
- [24] F. Cerdeira, T. Fjeldly, M. Cardona, *Phys. Rev. B* **1973**, *8*, 4734.

- [25] L. Brus, *J. Phys. Chem.* **1994**, 98, 3575.
- [26] C. Chartier, S. Bastide, C. Lévy-Clément, **2008**, *Electrochim. Acta* 53, 5509.
- [27] N. P. Dasgupta, C. Liu, S. Andrews, F. B. Prinz, P. Yang, *J. Am. Chem. Soc.* **2013**, 135, 12932.
- [28] K. Balasundaram, J. S. Sadhu, J. C. Shin, B. Azeredo, D. Chanda, M. Malik, K. Hsu, J. A. Rogers, P. Ferreira, S. Sinha, X. Li, *Nanotechnology* **2012**, 23, 305304.
- [29] M. Chandrasekhar, J. Renucci, M. Cardona, *Phys. Rev. B* **1978**, 17, 1623.
- [30] G. Pennelli, *Beilstein J. Nanotechnol.* **2014**, 5, 1268.
- [31] S. Jin, M. V. Fischetti, T. W. Tang, *J. Appl. Phys.* **2007**, 102, 083715.
- [32] M. T. Björk, H. Schmid, J. Knoch, H. Riel, W. Riess, *Nat. Nanotechnol.* **2009**, 4, 103.